Electronic Supplementary Material (ESI) for Physical Chemistry Chemical Physics.

Electronic Supplementary Information (ESI) to accompany:

Molecular photodissociation dynamics revealed by Coulomb explosion imaging

Stuart W. Crane,[1#] Jason W.L. Lee,[2] Michael N.R. Ashfold [1] and Daniel Rolles [3]

[1] School of Chemistry, University of Bristol, Bristol, U.K., BS8 1TS

[2] Department of Chemistry, University of Oxford, Oxford, U.K. OX1 3TA

[3] J.R. Macdonald Laboratory, Department of Physics, Kansas State University, Manhattan, KS 66506, U.S.A.

Figure S1

(a) Images of $H_xC_2Cl^{2+}$ (*m*/*z* ~31) fragment ions observed following 805 nm SFI of *cis*- (red borders) and *trans*-1,2-DCE at *I* = 260, 650 and 1300 TW cm^{-2}. **ε** is vertical in the plane of the image, as shown in the top left-hand panel, and the relative signal intensities for all but the central regions in the images – attributed to O_2^+ ions from SFI of trace air impurities – are shown by the linear false colour scale shown at the top right. (b) *P*(*v*) distributions of the $H_xC_2Cl^{2+}$ fragments from each parent isomer, with the low velocity contaminant feature plotted with a fainter pen. The maxima of the faster signal attributable to $H_xC_2Cl^{2+}$ ions formed from each isomer at each *I* has been scaled to unit intensity.

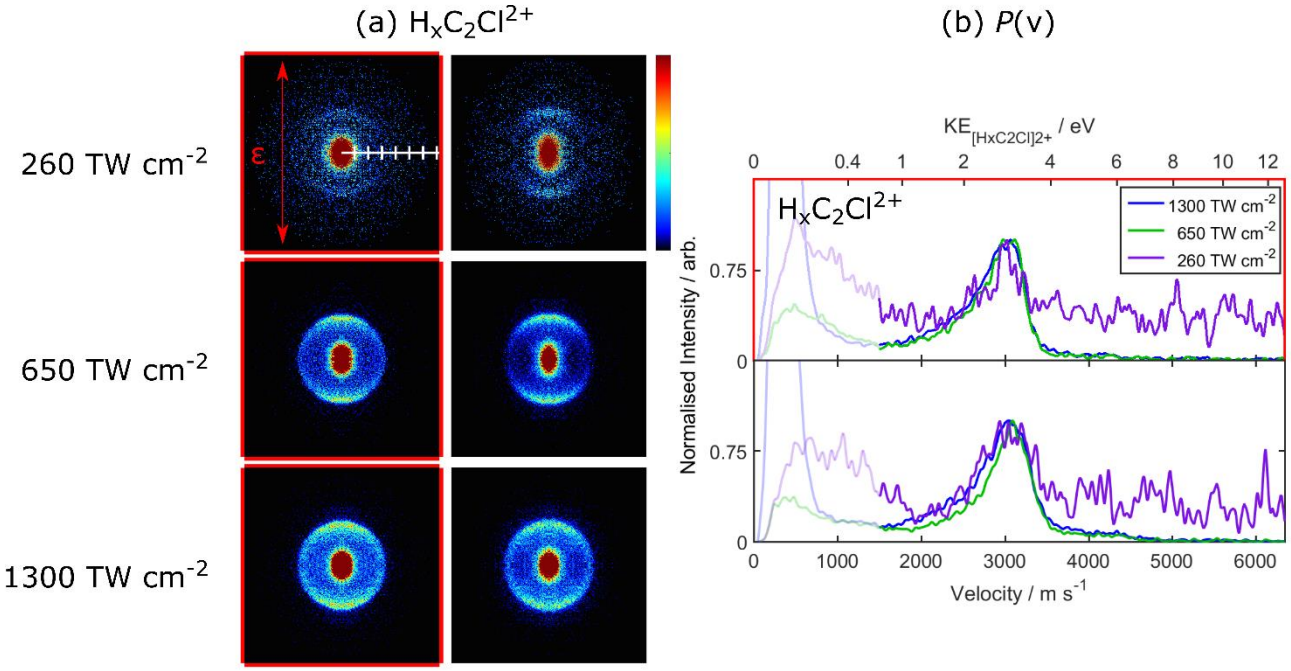

Figure S2

($C_2H_x^+$,Cl_2^+) and (Cl_2^+, $C_2H_x^+$) covariance map images from analysis of I = 260 TW cm^{-2} data from *cis*- (bounded in red) and *trans*-1,2-DCE, selecting the second listed species as the reference ion, fixing its velocity to be vertically upwards (as shown by the red arrow), and displaying the correlated 2-D velocity distribution of the counter fragment in the frame of the chosen reference ion. The intensity of the covariance signal attributable to process (7), bounded by dashed white lines and shown on a 2× expanded false-colour scale, is more intense in the case of the *cis*-isomer.

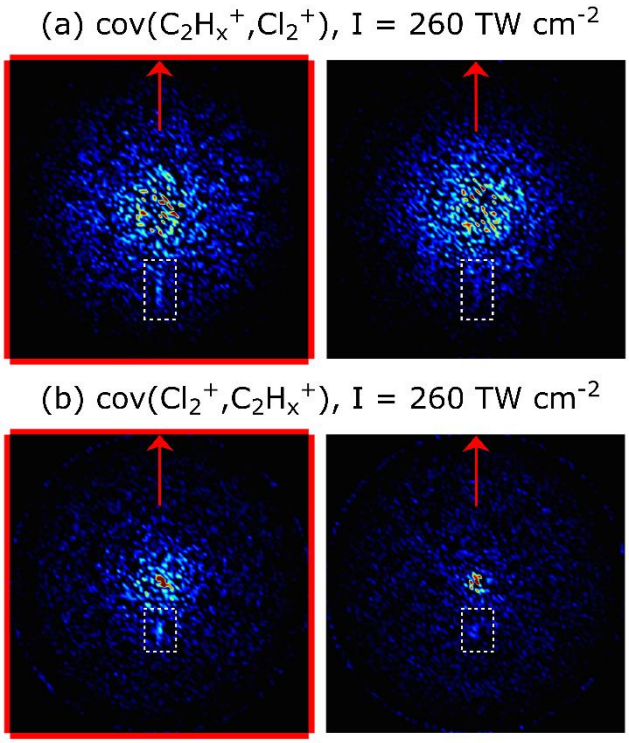

Figure S3

Symmetrised images of the CF_3^+, I^+ and I^{2+} fragments from ultrafast two-colour (267 nm pump – NIR SFI probe, I = 1300 TW cm^{-2}) studies of CF_3I at different time delays in the range –390 fs ≤ δt ≤ 1 ns prior to subtracting the corresponding one-colour NIR-SFI contribution. The **ε** vector of both laser beams is vertical, in the plane of the detector, as indicated by the double-headed arrow and the main NIR-only and two-colour channels are labelled with the acronyms defined in the text. The relative intensities in images displayed in any one row are depicted using a common linear false-colour scale spanning the maximum through minimum signal values shown at the far right of the top row. The corresponding images after subtracting the probe-only contributions are shown in Fig. 10.

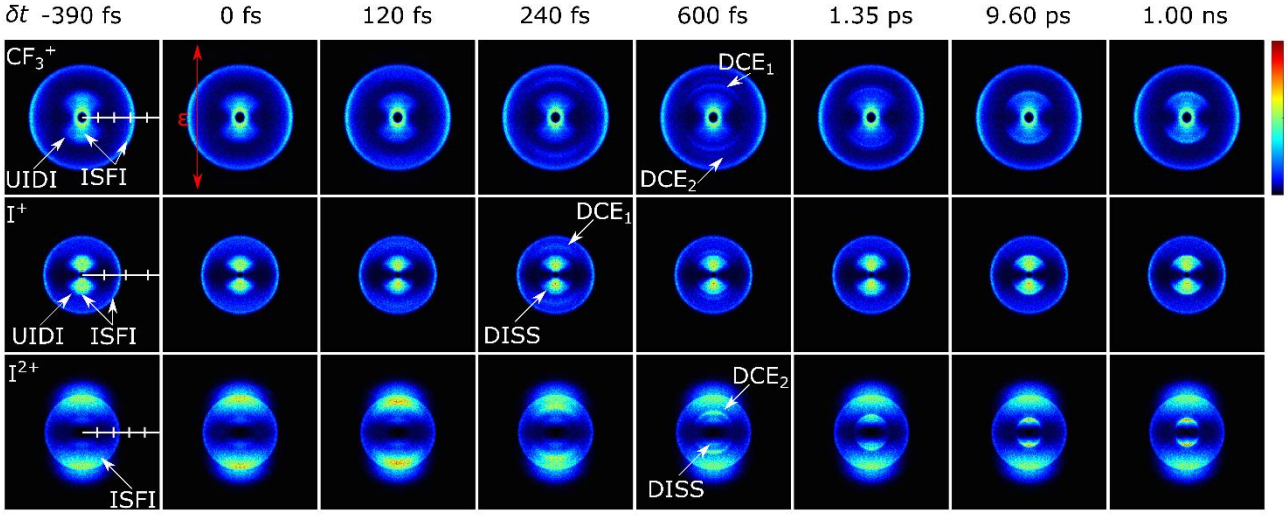

Figure S4

2-D false-colour maps showing the (a) CF_3^+, (b) I^+ and (c) I^{2+} ion velocities as a function of δ*t* obtained by angular integration of images measured following 267 nm photolysis of CF_3I and 805 nm SFI probing at I ~1300 TW cm^{-2} without subtraction of the NIR-only contribution, plotted using the linear false-colour relative intensity scale shown to the right of panel (b). The corresponding maps after subtracting the probe-only contributions are shown in Fig. 11.

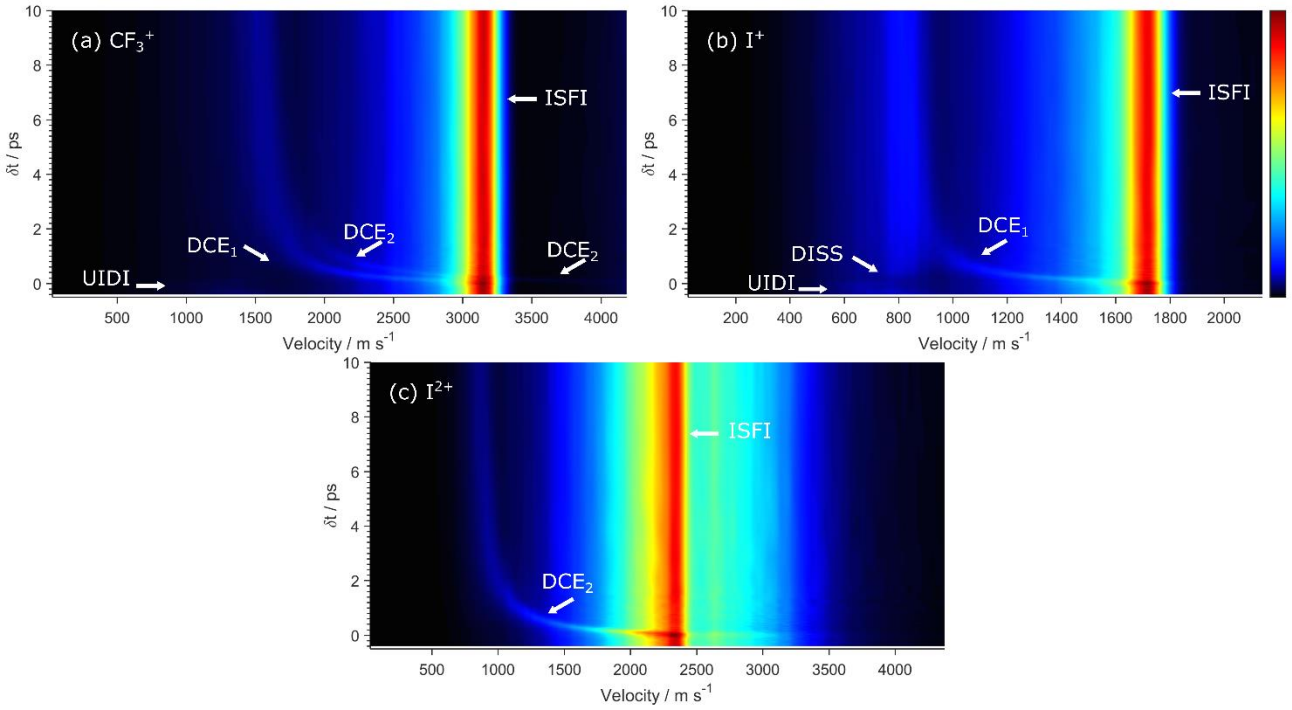

Figure S5

2-D false-colour maps showing the (a) CF_3^+, (b) I^+ and (c) I^{2+} ion velocities as a function of δt obtained by angular integration of images measured following 267 nm photolysis of CF_3I and 805 nm SFI probing at I ~650 TW cm^{-2}, after subtraction of an optimum fraction of the NIR-only contribution, plotted using the linear false-colour relative intensity scale shown to the right of panel (b). The various channels are labelled with the acronyms introduced in the text. (d) compares the $P(p)$ distributions of the CF_3^+, I^+ and I^{2+} ions at long time delays (δt ~1 ns) with the p values associated with primary photodissociation of CF_3I to ground (I) and spin-orbit excited (I*) atoms indicated, each normalised so that the CF_3 + I* feature appears with the same intensity.

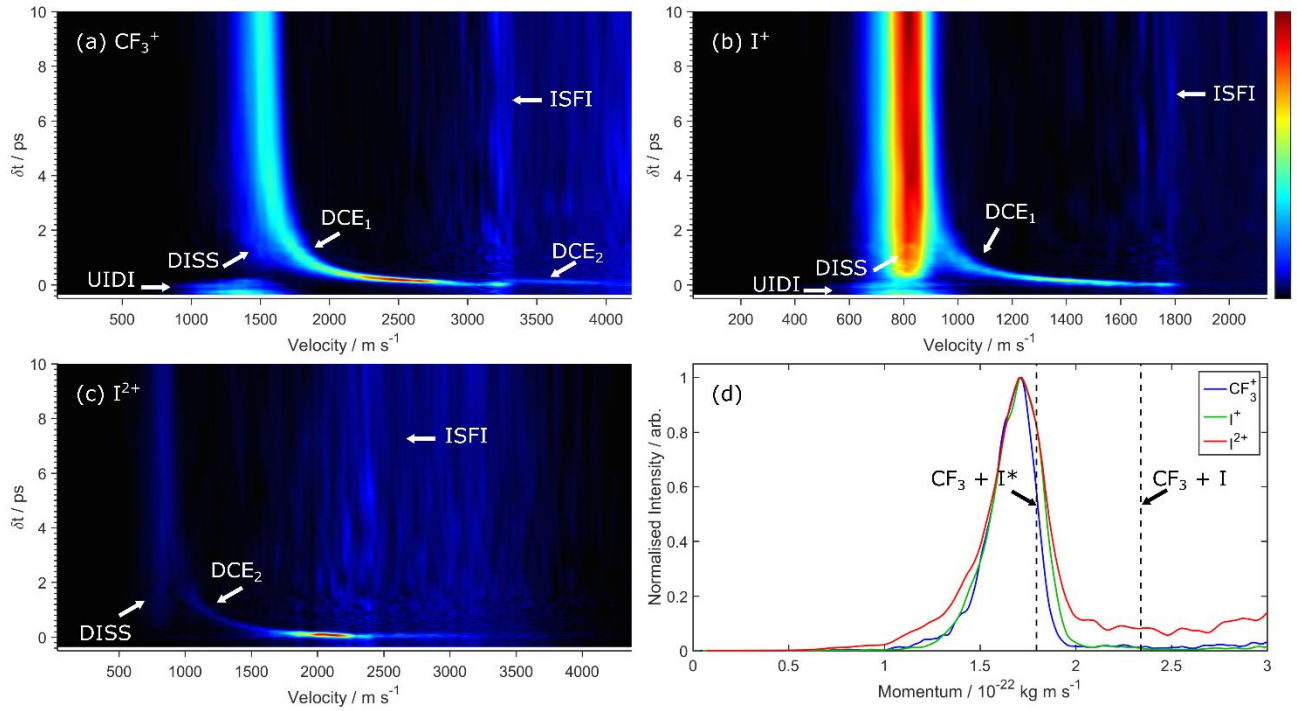

Figure S6

2-D false-colour maps showing the I^{3+} ion velocities as a function of δt obtained by angular integration of images recorded following 267 nm photolysis of CF_3I (panels (a) and (c)) and CH_3I (panels (b) and (d) and NIR SFI probing (I ~1300 TW cm^{-2}) after ((a) and (b)) and before ((c) and (d)) subtracting the NIR-only contribution. The relative intensities in each map are displayed using the linear false-colour scale shown to the right of panel (b). The DCE_3 features attributable to Coulombic repulsion between CX_3^+ (X = F, H) and I^{3+} ions formed by NIR-SFI of geminate CX_3 + I product pairs are clear in the upper plots.

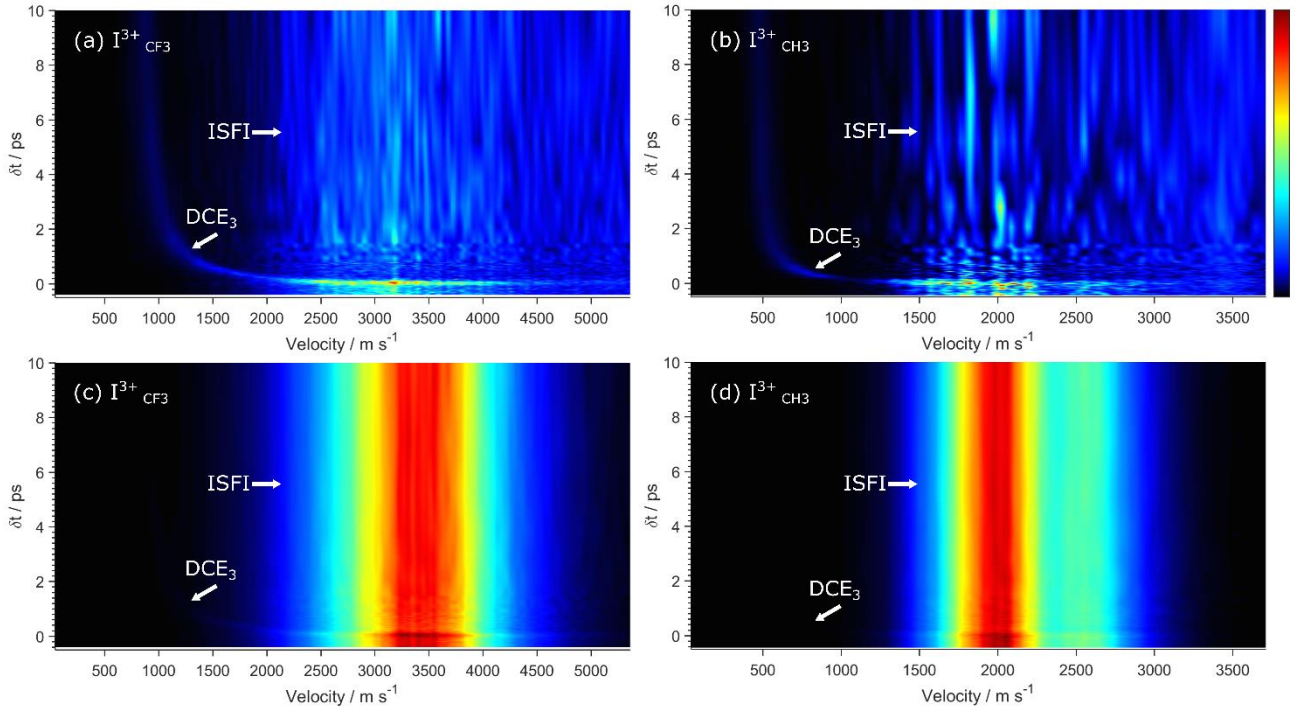

Figure S7

Symmetrised images of the CH_3^+, I^+ and I^{2+} fragments from ultrafast two-colour (267 nm pump – 805 nm SFI probe, I = 1300 TW cm^{-2}) studies of CH_3I at different time delays in the range -390 fs $\leq \delta t \leq$ 1 ns after subtracting the one-colour NIR-only contribution. The **ε** vector of both laser beams is vertical, in the plane of the detector, as indicated by the double-headed arrow. The relative intensities in images displayed in any one row are depicted using a common linear false-colour scale shown at the far right spanning the maximum through minimum signal values (left halves) and on a 10× expanded scale (right halves).

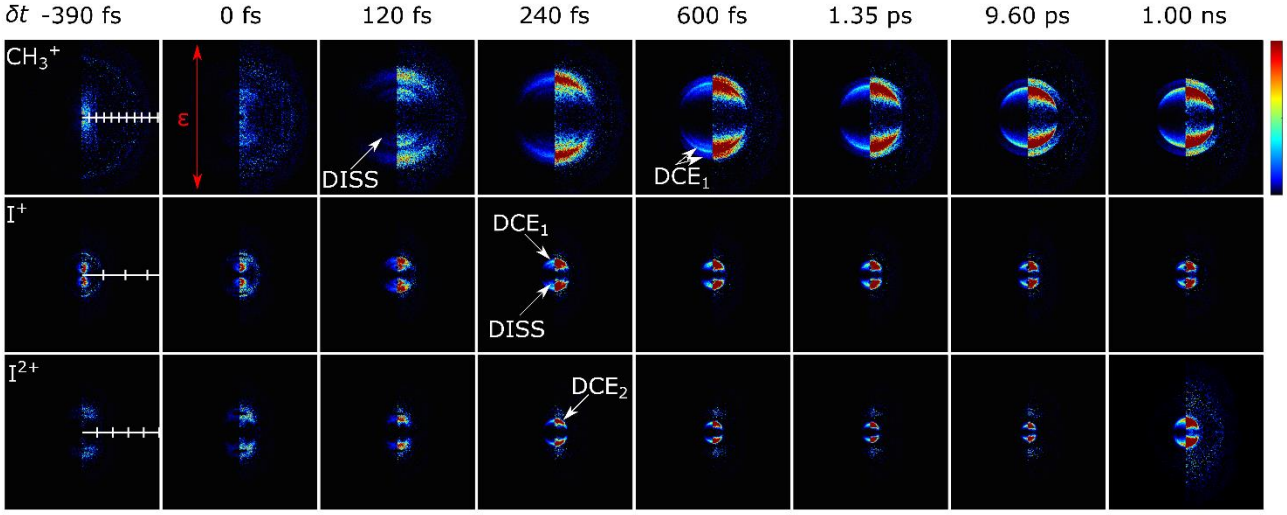

Figure S8

2-D false-colour maps showing the (a) CH_3^+, (b) I^+ and (c) I^{2+} ion velocities as a function of δt obtained by angular integration of the images recorded following 267 nm photolysis of CH_3I and 805 nm SFI probing at I ~1300 TW cm^{-2} without subtraction of the NIR-only contribution. Relative intensities are depicted using the false-colour scale shown to the right of panel (b). The corresponding maps after subtracting the probe-only contributions are shown in Fig. 13 of the paper.

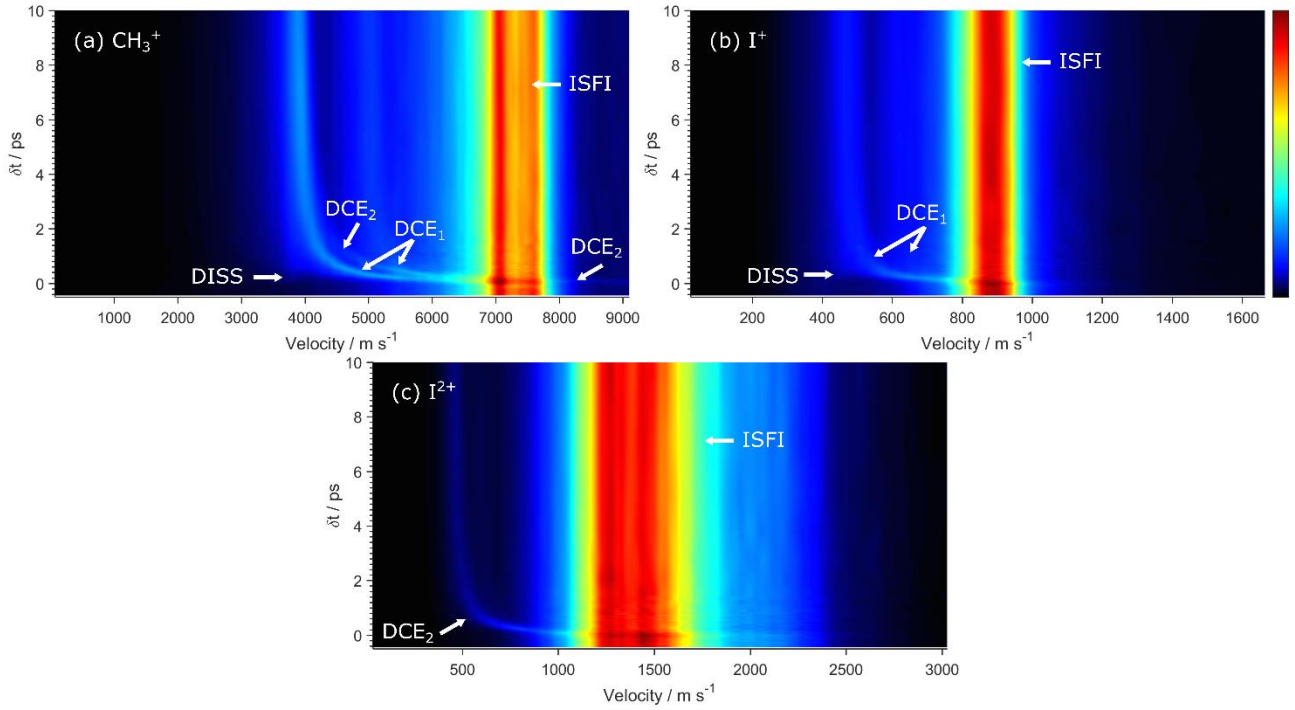

Figure S9

2-D false-colour maps showing (a) CH_3^+, (b) I^+ and (c) I^{2+} ion velocities as a function of δt obtained by angular integration of the respective images measured following 267 nm photodissociation of CH_3I and 805 nm SFI probing at I ~650 TW cm^{-2}, after subtraction of an optimum fraction of the NIR-only contribution. Relative intensities are depicted using the false-colour scale shown to the right of panel (b). The various channels are labelled with the acronyms introduced in the text. (d) Comparison of the $P(p)$ distributions of the CH_3^+, I^+ and I^{2+} ions obtained by integrating data measured over the delay range $0.1 \leq \delta t \leq 1$ ns, with the p values associated with primary photodissociation of CH_3I to ground (I) and spin-orbit excited (I*) atoms indicated. Each $P(p)$ distribution has been scaled so that the respective features associated with CH_3 + I* products have the same peak intensity.

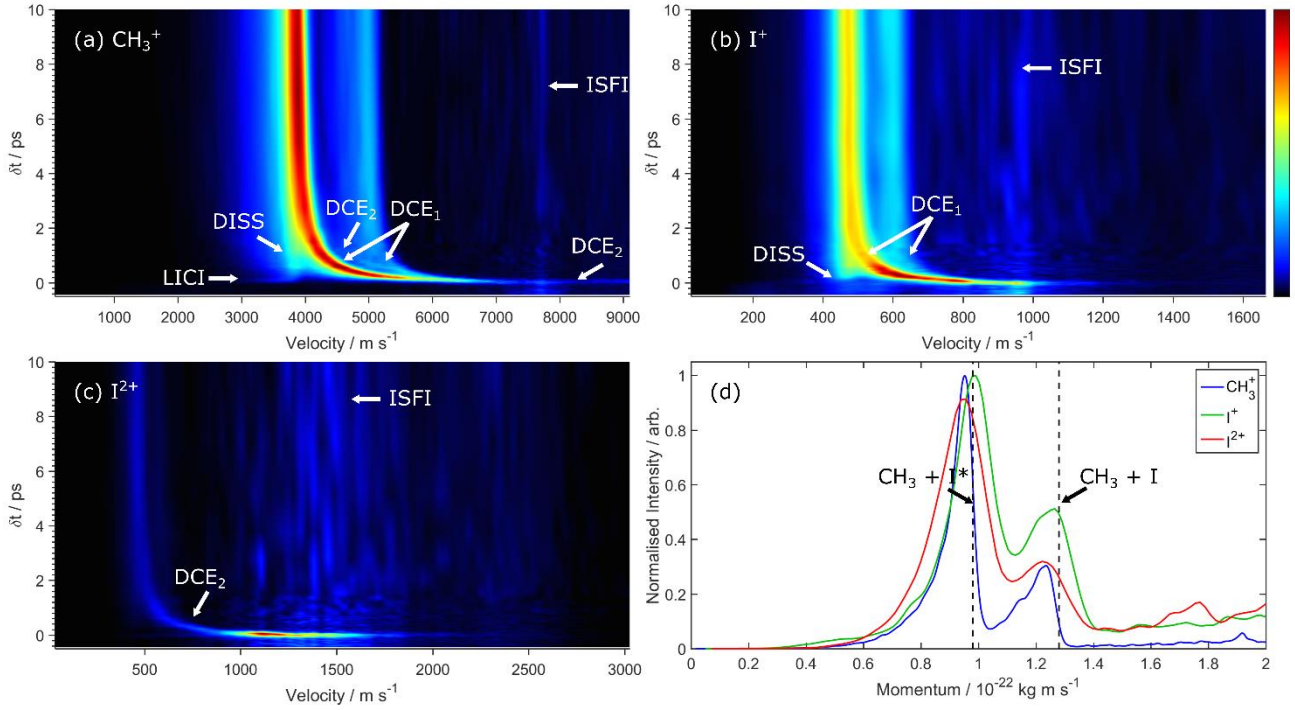

Figure S10

2-D false-colour maps showing (a) CH_3^+, (b) I^+ and (c) I^{2+} ion velocities as a function of δt obtained by angular integration of the respective images measured following 267 nm photodissociation of CH_3I and NIR probing at much lower intensity than that used when obtaining the data shown in Figs. S8 and S9 (I ~100 TW cm^{-2}) to accentuate the low velocity feature at δt ~0 (labelled LICI) in the CH_3^+ and I^+ maps. Again, much of the NIR-only contribution has been subtracted prior to display, relative intensities are depicted using the linear false-colour scale shown to the right of panel (b), and the various channels are labelled with the acronyms introduced in the text. (d): $P(p)$ distributions of the CH_3^+, I^+ and I^{2+} ions obtained by integrating data measured over the delay range $0.1 \leq \delta t \leq 1$ ns, with the p values associated with primary photodissociation of CH_3I to ground (I) and spin-orbit excited (I*) atoms indicated. Each distribution has been scaled so that the respective features associated with CH_3 + I* products have the same peak intensity.

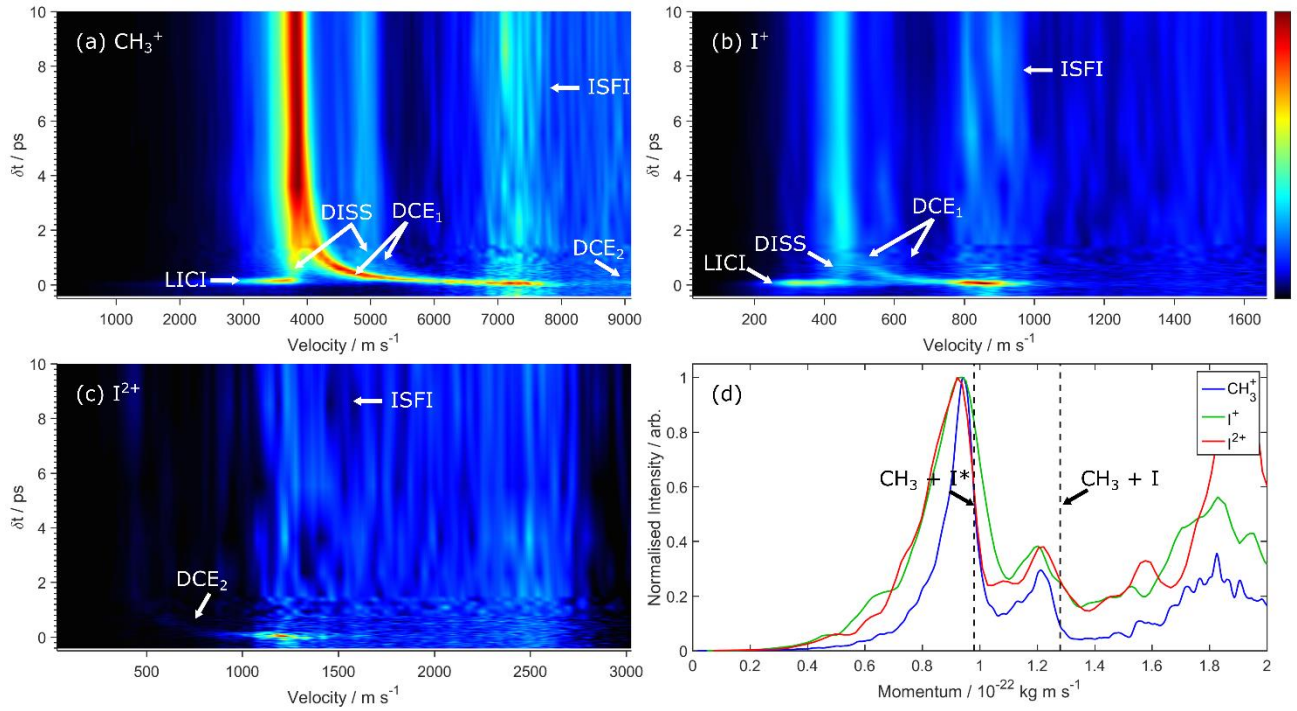

Figure S11

2-D false-colour maps comparing the I^{3+} ion velocities following 267 nm photolysis of CH_3I and probing with (a) an 11.5 nm XUV pulse and (b) 805 nm SFI at I = 1300 TW cm^{-2}, without subtracting the NIR-SFI one-colour contribution. The relative intensities in both panels are depicted using the linear false-colour scale shown to the right of panel (a).